Received: 1 December 2023 | Accepted: 22 June 2024

DOI: 10.1002/ppj2.20113

The Plant Phenome Journal OPEN ACCESS

ORIGINAL ARTICLE

High temporal resolution unoccupied aerial systems phenotyping provides unique information between flight dates

Jacob D. Washburn[1] | **Alper Adak**[2] | **Aaron J. DeSalvio**[3] | **Mustafa A. Arik**[2] | **Seth C. Murray**[2]

[1]USDA-ARS, Plant Genetics Research Unit, Columbia, Missouri, USA

[2]Department of Soil and Crop Sciences, Texas A&M University, College Station, Texas, USA

[3]Interdisciplinary Graduate Program in Genetics and Genomics, Department of Biochemistry and Biophysics, Texas A&M University, College Station, Texas, USA

Correspondence
Jacob D. Washburn, USDA-ARS, Plant Genetics Research Unit, 302-A Curtis Hall, Columbia, MO 65211, USA.
Email: jacob.washburn@usda.gov

Assigned to Associate Editor Michael Gore.

Funding information
Iowa Corn Promotion Board; Agricultural Research Service; National Institute of Food and Agriculture, Grant/Award Number: 2022-70412-38454

Abstract

Unoccupied aerial systems (UAS, unoccupied aerial vehicle, and drone) are high-throughput phenotyping tools that can provide transformational insights into biological and agricultural research, but practical and scientific questions remain. The utility of dense versus sparse temporal collections (e.g., daily, weekly, and monthly flights) has important implications for experimental design, resource allocation, and the scope of scientific questions investigated through UAS. UAS-derived image data were collected on over 1500 maize hybrid yield trial plots with a temporal (longitudinal, 4D) sampling density of 2.8 days on average between 43 flights throughout the growing season. Correlations of vegetation index (VI) phenomic features between flight dates were generally high between flights separated by only 1 or 2 days but dropped when 3, 4, or more days separated the flights. These varied depending on specific dates and the VI used. Correlations between flights were lower around flowering time than during other parts of the season indicating the phenotypic uniqueness of this developmental period. The cross-validation accuracy of end of season yields prediction models on untested genotypes from the UAS data (0.59 and 0.62) far exceeded genomic prediction accuracy (0.24) for the same test set hybrids regardless of whether all flight dates were used for prediction or only dates before flowering. Phenomic prediction accuracy marginally increased as additional flight dates were added throughout the season.

1 | INTRODUCTION

Falling costs, improved stability, and lowered barriers to entry have resulted in unoccupied aerial systems (UAS, unoccupied aerial vehicle [UAV], drone) becoming ubiquitous in various industries and among hobbyists. Where aerial phenotype data for agricultural plant breeding and research was once expensive and of low spatial and temporal resolution, it is now possible to collect high-resolution image data at a relatively low cost (Reynolds & Langridge, 2016; Sweet et al., 2022). The collection of high temporal resolution data, achieved by conducting flights many times throughout the growing season, is now feasible but comes with significant logistical, labor, data storage, and analysis considerations.

The usefulness of UAS data for predicting end of season phenotypes like yield is well demonstrated (Adak et al., 2023; Araus & Cairns, 2014; Danilevicz et al., 2021; Oehme et al., 2022; Rutkoski et al., 2016; Shi et al., 2016). This is

Jacob D. Washburn and Alper Adak contributed equally to this work.

particularly true for early flights that can provide breeders or producers with decision-making data earlier in the season (Danilevicz et al., 2021; Ma et al., 2001; Rutkoski et al., 2016; Yuan et al., 2019). Aside from yield prediction itself, aerial remote sensing data have been used successfully for monitoring and estimating disease (Herr et al., 2023; Mutka & Bart, 2015; Zhang et al., 2003), soil parameters, water stress (Zhang et al., 2019), and other factors (Singh et al., 2019; Tirado et al., 2021).

Temporal UAS or other remote sensing data have been collected across plant development in multiple studies and shown to be useful in predicting and understanding plant growth, yield, and other phenotypes (Adak et al., 2021a, 2023; Anderson et al., 2019; Krause et al., 2019; Oehme et al., 2022; Shi et al., 2016; Tirado et al., 2021; Wang et al., 2019). In general, each flight date in these studies appears to contain unique and useful phenotype information. It is now both theoretically and technically possible, weather permitting, to gather UAS data on the same field, or even multiple very large fields, every single day of the growing season (or even multiple times a day if desired). However, it remains unclear if such temporally dense data have scientific utility for plant breeding, development, physiology, or other disciplines, and at what point temporally close flights become functionally redundant. In other words, can flying more frequently help close the gap toward "saturating the phenome" (Murray et al., 2022), or at what point is there no extra information collected from day to day. While this seems primarily a question of fundamental biological discovery, it can also provide practical insights into the best periods to fly to predict phenotypes of interest. Some ideas can be gained from controlled environment automated imaging which collects such images daily (Fahlgren et al., 2015). However, to date, the densest reported flights of UAS over small plot genetic studies have been 23 across the season in maize (Tirado et al., 2021), but most studies have had fewer.

In investigating UAS applications to plant breeding, development, and physiology, it is also relevant to use a wide diversity of genetic material to ensure that variation in phenotypes is captured. Incorporating genetic diversity is especially important in UAS studies throughout time. For example, early-season development is typically not observed, has not been selected by breeders, and thus has been observed to have more predictive variation in breeding populations than the post flowering (Adak et al., 2021b). The Genomes to Fields (G2F) initiative is particularly rich in relevant genetic diversity and collects data on hundreds of maize hybrids in dozens of locations across the United States every year (AlKhalifah et al., 2018; Gage et al., 2017; Kick et al., 2023; Lawrence-Dill et al., 2019; Lima et al., 2023a,b,c; McFarland et al., 2020; Rogers et al., 2021; Washburn et al., 2021). Physiological traits, such as the leaf appearance rate, have also been shown to negatively correlate with yield under drought stress conditions and the opposite would likely be observed under water-sufficient conditions (Messina et al., 2011). These types of correlations could be better established and feasibly dissected with larger-scale studies using high-throughput phenomics.

Core Ideas

- Temporally dense unoccupied aerial systems (UAS) data contain unique information.
- Phenomic prediction outperformed genomic prediction.
- Temporal UAS data improved prediction accuracy.

In this study, we collected and analyzed temporally dense UAS phenotyping data at 43 flight dates across the season (on average 2.8 days between flights) from G2F hybrid maize field trials to determine the potential scientific and yield prediction utility dense temporal sampling might offer. We hypothesized that dense temporal UAS sampling would add value to both predictive modeling and biological understanding of how plants grow and develop over time, but that this marginal added value would likely decrease with each increase in sampling density. We had no a priori hypothesis as to how dense of sampling would be too dense to see any useful differences between flight dates, predictive accuracy, or biological interpretation. Thus, the underlying goal was to collect as much data as feasible.

2 | MATERIALS AND METHODS

2.1 | Field sites and manual phenotyping

Hybrid maize field trials were planted in two adjoining fields at the Bradford Research Center in Columbia, MO, in the summer of 2020 as part of the G2F (https://www.genomes2fields.org) Genotype by Environment Project. The trials were planted in a partially replicated design and consisted of 1107 genetically unique hybrids (with usable data for this project) spread over 1594 plots. Agronomic, management, soil, weather, and manual phenotype data were collected along with the trial. More specific details as well as the collected phenotype data can be found in the publicly available G2F data repository. Specific dependent phenotypes of interest used here include plant height (PHT), ear height (EHT), and combine-collected grain yield (yield) taken at the end of the season; as well as days to anthesis (DTA) and days to silking (DTS) recorded for each plot when 50% of the plants in the plot reached 50% of anthers shedding or silks visible. Anthesis-silking interval (ASI) was an additional phenotype calculated from DTA and DTS. Further details and

protocols on the collection of this data are documented in the G2F repository cited above.

2.2 | Field based high-throughput phenotyping and orthomosaic construction

Temporal phenomic data was collected using a DJI Mavic 2 Professional UAS (SZ DJI Technology). The UAS used a L1D-20c Hasselblad camera that records RGB imagery at 20-megapixel resolution with a 1-inch CMOS sensor and electronic shutter ranging between 8–1/8000s. Raw RGB imagery was sorted into separate folders named according to each flight date in preparation for construction of orthomosaics within Agisoft Metashape (Agisoft LLC). A summary of orthomosaicking and georeferencing procedures is described as follows: (a) folders containing RGB images were loaded into Metashape; (b) photo alignment was conducted using 40,000 key points and 4000 tie points with referenced preselection; (c) an initial bundle adjustment was performed to optimize the f, cx/cy, k1, k2, k3, p1, and p2 distortion parameters of the lens; (d) iterative model error reduction procedures (termed "gradual selection" in Metashape) were performed to remove erroneous points from the sparse cloud; (e) ground control points (GCPs) were imported and manual alignment of their locations within at least six RGB images was performed followed by selecting the "update" option within Metashape to integrate the GCPs into the model; (f) camera alignment was performed again with all available distortion parameters; (g) the dense point cloud was processed with "moderate" depth filtering at "medium" quality with all other settings left as default; (h) color calibration was performed using the sparse cloud as the source and the "calibrate white balance" option was also checked; (i) the digital elevation map (DEM) was calculated using the dense cloud as the data source with all other settings left as default; (j) the orthomosaic was produced using the DEM as the surface with all other settings left as default. All georeferenced final products were exported in World Geodetic System 1984 (WGS84) datum (specifically, UTM Zone 15N) coordinates due to the flights occurring in Columbia, MO. Orthomosaics and DEMs were exported from Metashape and saved with the .tif extension, while the dense point cloud was saved with both .las and .laz file extensions. PHT data were extracted on a plot basis using the .laz point cloud.

2.3 | Phenomic data extraction

In total, 36 vegetation indices (VI) and PHTs were extracted for each row plot in each orthomosaic and their names, formulas, and citations can be found in Table S1 (Bendig et al., 2015; Burgos-Artizzu et al., 2011; Gitelson et al., 2002; Golzarian & Frick, 2011; Guerrero et al., 2012; Guijarro et al., 2011; Hague et al., 2006; Hunt et al., 2005, 2011; Kataoka et al., 2004; Louhaichi et al., 2001; Meyer & Neto, 2008; Meyer et al., 1999; Richardson & Wiegand, 1977; Tucker, 1979; Woebbecke et al., 1995; Zarcotejada et al., 2005). Briefly, (i) plot-based shape files (polygons) were created using the *UAStools::plotshpcreate* (Anderson & Murray, 2020). (ii) *FIELDimageR::fieldMask* was used to remove the background soil in each orthomosaic so as not to confound measures of plant health with canopy cover.(iii) *FIELDimageR::fieldIndex* was used to calculate the value of each VI for each row plot (Matias et al., 2020). Weibull fit analysis was used to temporally smooth the PHT data and remove errors due to poor point cloud accuracy and other inherent challenges with extracting PHT from UAV image data (Anderson et al., 2020).

2.4 | Statistical modeling of variance components and best linear unbiased estimators and predictors (BLUEs and BLUPs)

A BLUP model, similar to that described in Adak et al. (2023) to calculate the genotypic effects across flight times, is given as:

$$y_{ijklm} = \mu + H_i + F_j + HF_{i\times j} + \text{range}_k + \text{row}_l + \text{rep}_m + \varepsilon_{ijklm}$$

Here, y_{ijklm} is the value of a VI belonging to ith hybrid in kth range (also known as column), lth row, mth replication at jth flight date; $H_i \overset{\text{iid}}{\sim} N(0, \sigma^2_{H_i})$ is the random effect of hybrid with $i = (1, \ldots, 1107)$; $F_j \overset{\text{iid}}{\sim} N(0, \sigma^2_{F_j})$ is the random effect of flight date for the 43 flights as days after plating treated as factor with j = (9, 10, 15, 17, 22, 24, 27, 30, 32, 34, 37, 39, 41, 45, 48, 51, 53, 56, 60, 62, 64, 66, 69, 71, 73, 76, 78, 80, 83, 87, 90, 93, 96, 99, 101, 104, 107, 111, 114, 118, 122, and 126); $HF_{i\times j} \overset{\text{iid}}{\sim} N(0, \sigma^2_{HF_{i\times j}})$ is the interaction effect between ith hybrid and jth flight date; range_k, row_l, and rep_m are the effects of kth range, lth row and mth replication effects with $\text{range}_k \overset{\text{iid}}{\sim} N(0, \sigma^2_{\text{range}_k})$, $\text{row}_l \overset{\text{iid}}{\sim} N(0, \sigma^2_{\text{row}_l})$, and $\text{rep}_m \overset{\text{iid}}{\sim} N(0, \sigma^2_{\text{rep}_m})$, respectively. ε_{ijklm} is the unexplained error. This model was used to generate BLUPs for each VI and UAS-derived Weibull fit PHT at each flight date, and the manually measured phenotypes PHT, EHT, yield, DTA, and DTS. Random effects models were also used for variance components for hybrid, flight, hybrid:flight, range, row, and rep. Repeatability, Rsquared, and the coefficient of variation (CV) were also calculated for each phenotype. Repeatability in this case was calculated using the same equation as heritability but called repeatability since the genetic material is not a structured population. BLUPs were used because flights were considered to be sampled randomly from

TABLE 1 Prediction models and their notations.

Model	Notation
M1 (genomic prediction)	$y = \mu + A + D + \varepsilon$
M2 (full-season 43 flight phenomic prediction)	$y = \mu + P_1 + \varepsilon$
M3 (pre-flowering 14 flight phenomic prediction)	$y = \mu + P_2 + \varepsilon$

a distribution of all possible flights. BLUEs were used in the yield prediction models because, in this case, specific hybrids in specific locations were selected as being of interest and considered fixed effects. Between flight Pearson correlations were calculated from the BLUPs as well as autocorrelations across the season (correlations between groups of flight dates that differed by a given number of days [e.g., 1 day, 2 days, and so on]).

2.5 | Prediction models

For the prediction models, phenotypic BLUEs for grain yield from the 1107 hybrids were used in both genomic and phenomic predictions. In genomic prediction, additive (A) and dominance (D) relationship matrices were created using 304,687 markers coded as 0, 1, and 2 in the AGHmatrix package in R (Amadeu et al., 2016; VanRaden, 2008; Vitezica et al., 2013). Two types of relationship matrices were developed for the phenomic prediction models according to VanRaden (2008). The first phenomic relationship matrix was the $P_1 \sim N(0, \frac{PP'\sigma^2_{p_1}}{37 \times 43})$, where P_1 is the phenomic relationship matrix derived from the 36 VIs and PHT for all 43 flights, and $\sigma^2_{p_1}$ is the respective variance components. The second phenomic relationship matrix was the $P_2 \sim N(0, \frac{PP'\sigma^2_{p_2}}{37 \times 14})$, where P_2 is the phenomic relationship matrix derived from the 36 VIs and PHT belonging to the first 14 flights, from 9 to 45 days after planting (DAP), that were before onset of flowering time, and $\sigma^2_{p_2}$ is the respective variance components. Prediction models are given in Table 1. Phenomic data were an $n \times q$ matrix, where n was the number of hybrids and q the temporal measurements. The relationship matrix was calculated to obtain the variance-covariance matrix structures as $n \times n$ for both phenomic and genomic BLUP (additive and dominance genomic relationship matrices) in the prediction model (de los Campos et al., 2009). Fivefold with 25 repeats cross validation was applied to prediction models. Fourfolds were used as training data while onefold was used as a test or hold-out data set for evaluating the performance of the model. Hybrids in the fourfold and onefold data sets were denoted as the tested and untested hybrids, respectively. Prediction ability (Pearson r in this article) was calculated between observed and predicted values of untested hybrids. This testing scenario is similar in overall concept to what has been described as "CV1" but there are important differences such as its calculation for a single environment and its use in predicting late-season phenotypes from early-season phenotypes rather than genetics. For these reasons, we describe our testing scenario as "CV1-like" (Burgueño et al., 2012).

Additional phenotypic prediction models were created exactly as above but using a unique model for each flight date and all those before it. These models were progressive across the season so that the first flight date model only included the first flight date data (37 VIs × 1 flight), the second flight date model included the first and second flight dates (37 VIs × 2 flights), the third model included first, second, and third flight dates (37 VIs × 3 flights), and so forth (see code repository scripts for exact functions used). To determine if accuracy differences between models were statistically significant, an analysis of variance and Tukey's honestly significant difference (HSD) tests were performed. The Python implementation of Tukey's HSD in the statsmodels package was used, including the Tukey's HSD multi-comparison function (Hochberg & Tamhane, 2009). Since the Weibull fit PHT uses data from multiple flight dates to adjust each individual flight date's PHT phenotype, models were run both including and excluding it. In the end, the results were similar regardless of PHT inclusion. Improvements due to PHT were seen for some models but these occurred even in the final model with all dates included, indicating that leakage of data across flight dates was minimal if it occurred at all. For this reason, the prediction models with Weibull fit PHT included were used throughout the manuscript.

The scripts used in the analyses and figure generation for this manuscript are available at https://github.com/JacobWashburn-USDA/dense_UAV. Both the scripts and phenotypic tabular data needed to recreate the analyses are available at https://doi.org/10.5281/zenodo.11085557.

3 | RESULTS

3.1 | Correlations and autocorrelations between flights decrease after a few days of separation

Principal component analysis grouped many of the VIs together indicating that some indices such as the normalized green red difference index (NGRDI), visible atmospherically resistant index (VARI), and green minus red index (GmR) cluster together and likely contain similar information while others such as the normalized difference red blue index (NDRBI), red minus blue index (RmB), and blue chromatic coordinate index (BCC) are more distinct or form their own clusters (Figure S1). While these groupings were helpful in exploring and prioritizing different indices for analysis, most analyses were run on all VIs for comprehensiveness.

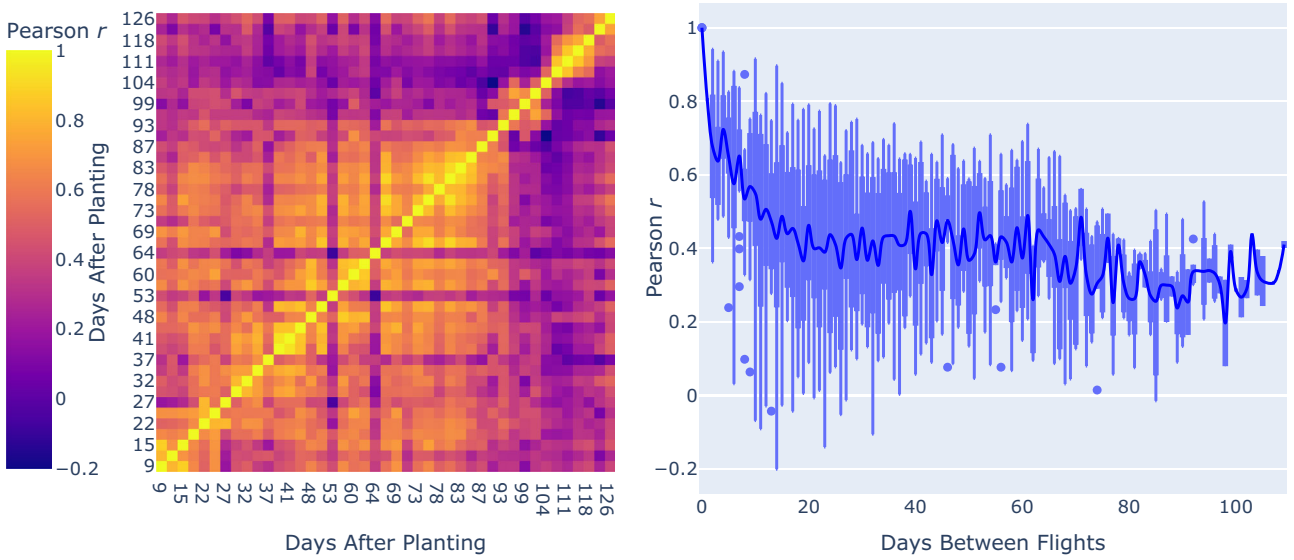

FIGURE 1 RmB vegetative index correlations and autocorrelations between (A) flight dates throughout the season and (B) autocorrelations for all pairs of flights and every possible distance between flights across the season in days.

Pearson correlations between flight dates varied substantially depending on the VI examined and the point in the season at which the flight was conducted. This was also the case for autocorrelations with the number of days between flights having a strong impact for many of the VIs. Some Vis such as VARI and NGRDI had relatively high correlations (Pearson $r > 0.7$) between flight dates throughout the season while others such as RmB had a range of correlations varying from nearly perfect to negative correlations depending on the flight dates compared (Figure 1A and Figures S2 and S3). Similar results were seen regardless of if DAPs (Figure 1) or growing degree days were used (Figure S2). Flights later in the season (after 90 days) showed lower correlations than the rest of the season. This is likely due to plant senescence in the later part of the season. Autocorrelations (between all flight dates separated by a given number of days, e.g., all pairs of flights separated by 1, 2, or more days) showed high correlations for flights separated by only a few days and lower correlations as the number of days between flights increased. Figure 1B shows one of the more extreme VIs (RmB) in this regard, but many other VIs follow similar patterns, while several VIs show almost no decrease (Figure S4). In most cases, the magnitude of change was largest when moving from flights separated by 1 day to those separated by 2 or 3 days.

Correlations between the various VIs and manually collected phenotypes show a diversity of patterns depending on the phenotype, VI, and flight date examined (Figures S5 and S6). The highest Pearson *r* correlations for any single flight were 0.52 for yield, 0.67 for PHT, 0.51 for EHT, 0.38 for DTA, and 0.37 for DTS. In general, correlations with yield, PHT, and EHT were fairly consistent or increased with time throughout the season with a steep drop off toward the end of the season (Figure 2 for VI GmR, Figure S6 for all VIs). EHT/PHT was also calculated and showed lower correlations than EHT or PHT alone (Figure S5). For many VIs, DTA and DTS showed stronger correlations in the middle of the season around the time of flowering than in other parts of the season; however, there was significant variation in the patterns seen in different VIs (Figure S6). The average flowering times from manually recorded DTA and DTS values across all hybrids were 52 and 53 DAP, respectively.

3.2 | Temporal PHT, manual phenotypes, and variance components

PHT is one of few traditional manual phenotypes that can be easily abstracted from UAV imagery. However, the accuracy of image-derived PHT measurements can be impacted by flight conditions and other factors including the resolution of the images, overlap between images, quality of point cloud reconstruction, and others making the height values of individual flights extremely variable. A Weibull fit model was used to temporally smooth the PHT data (see Section 2, Figure 3A). Phenotypes derived from the temporal PHT curve, as well as manual phenotypes, are displayed in Figure 3B. The variance components analysis of temporal PHT indicated that most of the variation could be explained by differences between flight dates (Figure 3C and Figure S7) as might be expected given the significant changes in PHT seen across development. The use of descriptive statistical phenotypes derived from the temporal PHT curve increased the variation that could be explained by hybrid (genetics) but still most of the variance was explained by experimental design

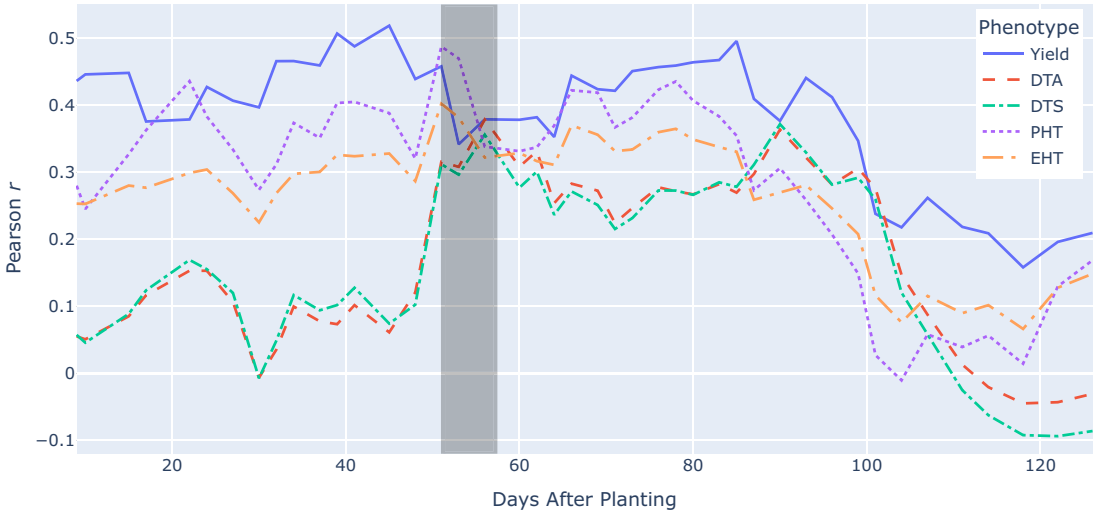

FIGURE 2 Correlations between standard manual phenotypes taken for each plot at a single time point in the season and the vegetative index GmR from flights throughout the season. The few days before and after the average flowering time are highlighted with a gray box.

factors or error. Of the traits examined, DTA, DTS, and EHT had the largest variance component attributable to hybrid. This hybrid variance is likely at least partially explained by plant phenology, but since phenological traits such as DTA and DTS are highly heritable in maize, distinguishing between the genetics unique to these traits and genetics of overall phenology is challenging.

Variance component analyses of VIs were conducted to better understand the contributions of different factors to the temporal VI values. When multiple flights were considered in a single model the factor for flights was always the largest variance component, as it was for PHT above, in many cases accounting for over 90% of the total experimental variation (Figure S8). Some VIs like NDRBI had higher residual variance components than others, while other indices like GmB had higher relative contributions from hybrid (genetics) by flight interactions. Removing the flight component by considering each date individually allowed a deeper investigation into other components. Depending on the VI used, hybrid accounted for between 0% and 44% of the variation with the highest percentages seen around and after flowering (Figure 4). Experimental design factors such as row, range, and replicate also accounted for significant portions of the variance.

3.3 | Genomic prediction compared with phenomic prediction

To better understand the usefulness of high temporal resolution data, grain yield was predicted using three different models. Phenomic models (M2 and M3) predicted grain yield better than genomic prediction (M1) for untested genotypes. The phenomic prediction model that used all VIs and Weibull fit heights belonging to all flight times (M2) predicted grain yield better on hidden (e.g., untested) genotypes than any of the other models (0.62 ± 0.04; Figure 5). The phenomic prediction model that used only VIs and heights belonging to flight times before flowering (M3) was the second-best model for predicting grain yield (0.59 ± 0.05). The genomic model predicted grain yield with the lowest accuracy (0.24 ± 0.06) for previously unseen hybrids.

3.4 | Genomic prediction compared with phenomic prediction over time

To better understand the usefulness of each additional flight date throughout the season in predicting yield, we created and tested a series of phenomic prediction models within a CV1-like scenario (most relevant scenario to breeding). The models were run both with and without Weibull fit PHT data included out of concern that the Weibull fit might create data leakage between flight dates and result in an overestimation of accuracy. However, the results were very similar and no indication of data leakage was found, so the version with height data included was used for all further analyses. The version excluding height data can be found in Figure S9. Each model used VI data from a given flight date in the season and from all previous flight dates. For example, the first model was based on only the first flight date, the second model was based on the first and second flight dates, and so forth to the last flight date of the season (Figure 6). This is relevant to a field program where data can constantly be updated throughout the season with the additional UAS data collected. All phenomic prediction models outperformed the genomic prediction model in cross-validation estimation of unknown genotypes. In general, these phenomic

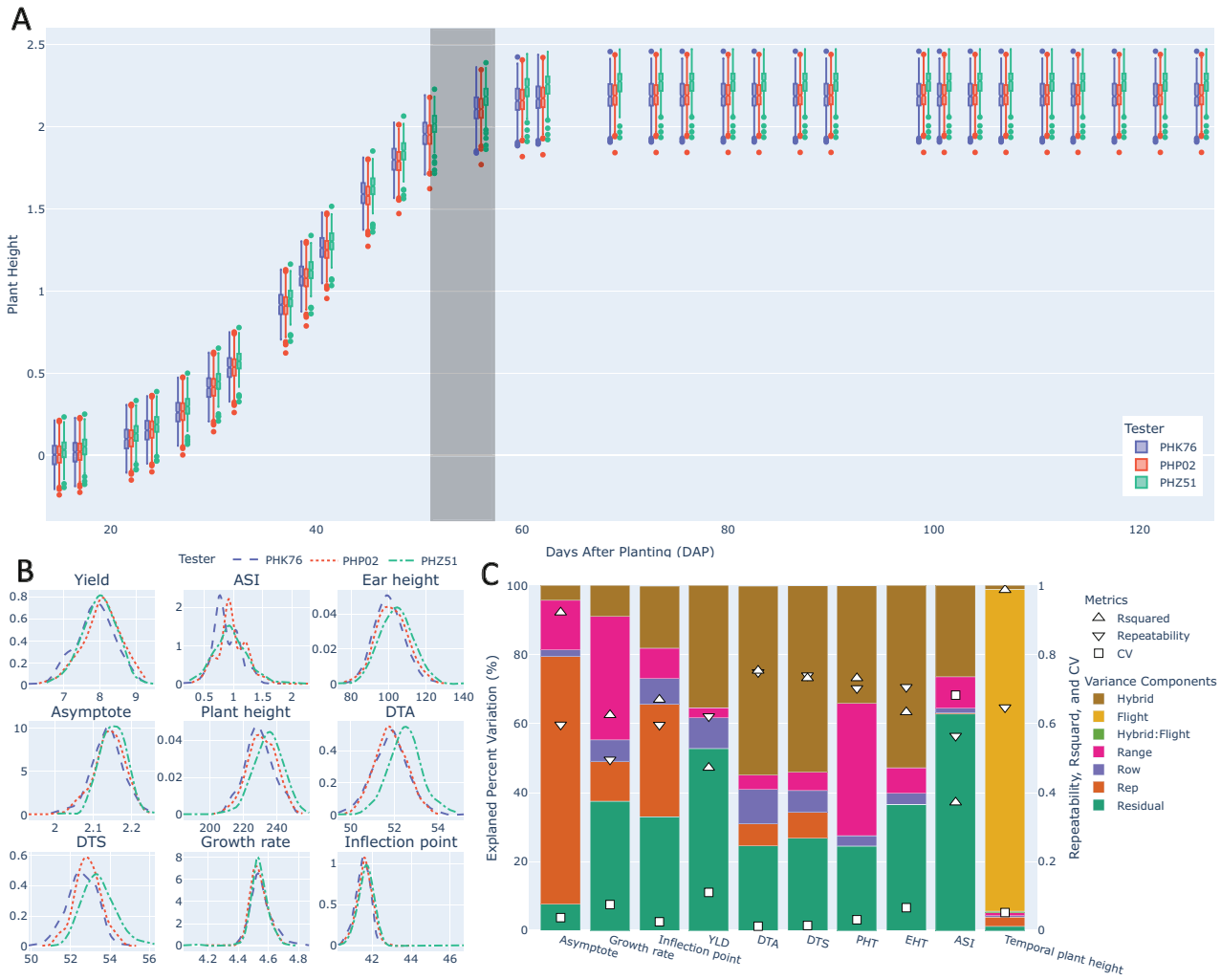

FIGURE 3 (A) Temporal plant height after Weibull fit modeling shown by tester. Gray box represents the mean flowering time plus and minus the standard deviation. PHK76, PHP02, and PHZ51 are the names of tester inbreds used in the study. (B) Densities of phenotype values by tester for manual phenotypes including days to anthesis (DTA), days to silking (DTS), anthesis silking interval (ASI), plant height (PHT), ear height (EHT), and grain yield as well as descriptive phenotypes derived from the Weibull fit temporal plant height data including asymptote, inflection point, and growth rate. (C) Percent variance explained by both manual and temporal plant height phenotypes. Variance components were derived from the BLUPs model described in Section 2.4. Temporal plant height was derived from a similar model but with Weibull fit height as the phenotype.

prediction models improved with the addition of more flight dates throughout the season. For a short time window in the early part of the season, some of the models decreased marginally in accuracy; with the addition of more flights, this trend was reversed for the rest of the season. Potentially useful, but not statistically significant improvements were seen throughout the season. Statistically significant improvements (Tukey's HSD, alpha = 0.05) over the first flight date model occurred in all models that included data from 39 or more DAP. The pattern seen in Figure 6 with prediction accuracy increasing in steps and plateaus rather than a continuous increase throughout the season may be biologically meaningful in some cases, but could also be an artifact of each flight or the way plots were manually delineated (according to the current standards) on the orthomosaic images of each flight date. Since orthorectification and mosaic software are not perfectly accurate and plants can blow in the wind, grow to the side, or otherwise change their exact location in the field marginally throughout the season, the delineation of plot boundaries was checked and updated between each flight. While every effort was made to accurately update plot boundaries, small inaccuracies are more likely to be missed, leading to moderate decreases in accuracy, and then corrected when they become large enough to be noticeable to the human eye, resulting in a jump in accuracy.

4 | DISCUSSION

The results indicated that flights over the same field from only a few days apart can contain unique information with the potential to improve our understanding and prediction of plant

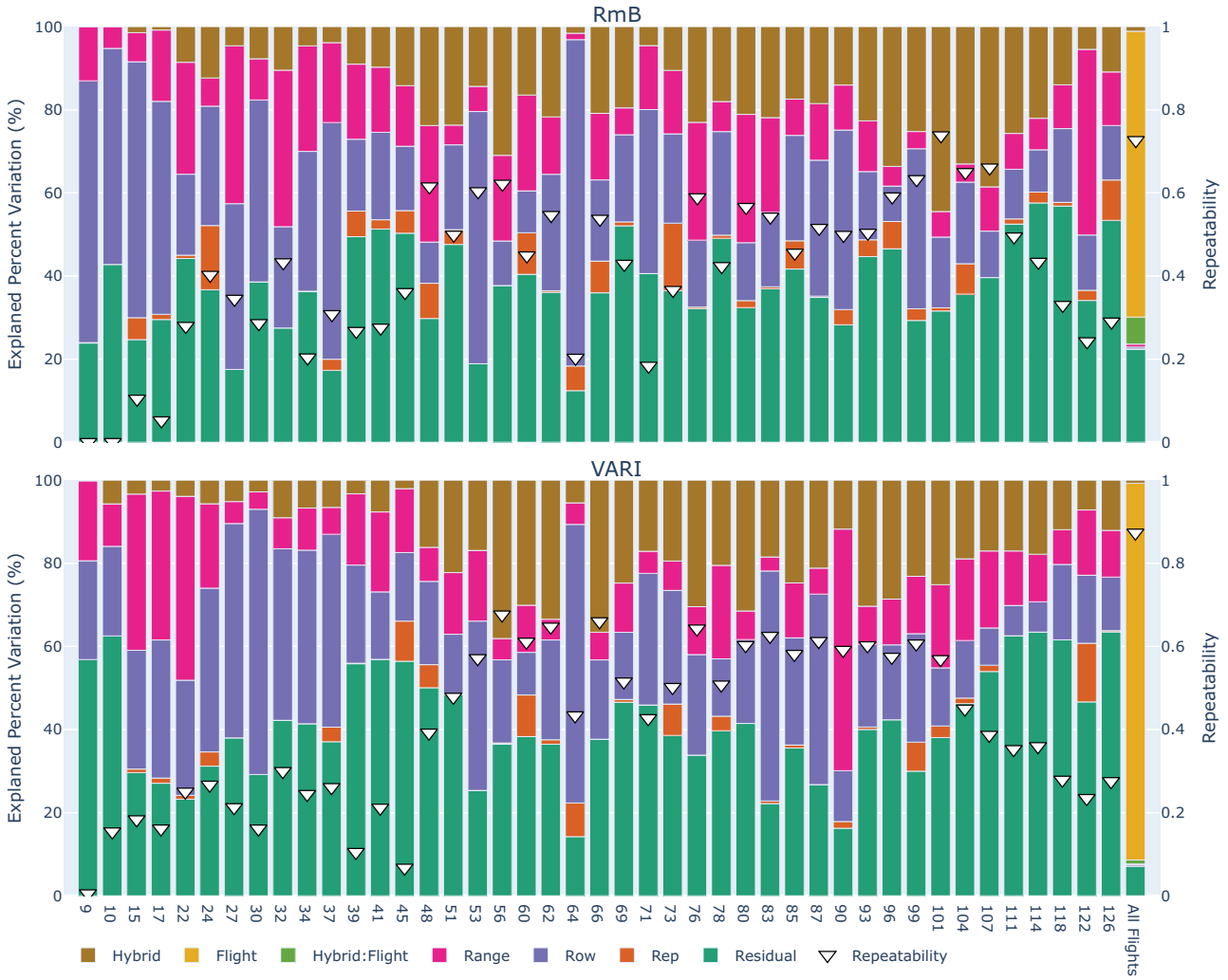

FIGURE 4 Variance components and repeatability for the VARI and RmB vegetative indices for each flight date individually and all flight dates together (far right).

development in the field over time; however, this is not true for all VIs examined as some have high autocorrelation across the season regardless of the number of days between flights. The reasons for this drop in autocorrelation are unclear but it appears that some VIs are better at differentiating between flight dates than others. The unpredictability of weather is one potential explanation for these rapid drops in correlation. Even if the plants themselves are not changing much over the course of a few days, changing weather could have considerable impacts on the appearance of the plants. A second explanation is varying data quality from each flight, as artifacts can be introduced for any single date in image capture, orthomosaic construction, and plot extraction. None of the flights were performed during high winds or rain and the majority took place on very clear sunny days around the time of solar noon, which should mitigate many weather-related changes. The concurrent increase in DTA and DTS with a decrease in yield for many of the VIs is an interesting pattern. DTA and DTS increases make sense given that they are flowering time traits, but an explanation for the drop in autocorrelation of VIs around flowering time with yield is less clear. The fact that early or delayed flowering can cause significant reductions in yield is one potential explanation. Another is that a saturation of response occurs around this time.

The usefulness of these data in predicting end of season phenotypes more accurately than genomic prediction is also clear and in agreement with previous studies comparing genomic and phenomic prediction (see introduction). However, in the context of yield prediction, accurate results could be obtained from our data without the high temporal sampling density used here (Figure 6). In fact, the greatest increase in accuracy over genomic prediction that we observed came from the very first flight in the data set, which was collected nine DAP and was not surpassed statistically until 39 DAP and that only by a small margin. One explanation for this might be that plants with rapid and consistent emergence are able to establish more uniform canopies, which could lead to more synergistic competition between plants and higher

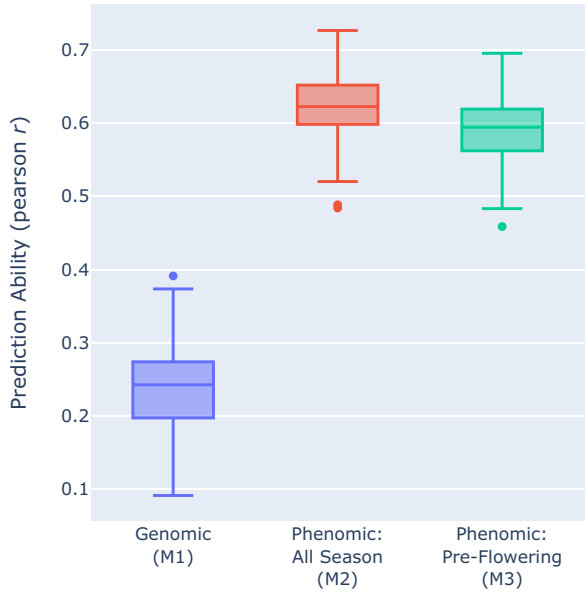

FIGURE 5 Prediction ability results from predicting yield using genomic prediction and two different phenomic prediction models: one with all flight dates, the other with only flight dates before flowering. The phenomic models included all calculated vegetative indices as well as UAS derived Weibull fit plant height. All predictions were made using a CV1-like data splitting scenario by holding out (e.g., hidden or untested) a subset of genotypes.

yields. Another bump in accuracy is seen around 78 DAP and this might be explained by environmental and physiological processes including ear competition (Messina et al., 2019). In our opinion, a substantial portion of the accuracy advantage over genomic prediction could be attributed to UAS data better accounting for plant health, vigor, and possibly heterosis through VIs. Because the soil was excluded in calculating these VIs, plot biomass traits such as stand count, plant density, and leaf area likely did not play a role.

Given the results, a logical question might be why expend the resources to fly and process data dozens of times throughout the season? From a practical standpoint, one reason to make additional flights is the unexpected random error in each flight. UAS flights and data processing over small plots still remain part art and luck and part science and engineering. Across different studies, we have frequently found flights that produce poor image quality or orthomosaics that must be dropped from the analysis. It is also not yet possible to predict what type of environment will exist as the plants grow and there have not been enough studies reported to dissect the causes of differences, especially across locations. Furthermore, this study relied on a single location with fairly limited stressors throughout the season. This very predictable and low-stress environment may be one reason that flights during the vegetative stage remained so predictive of end of season yield. In environments with more significant heat or drought stress (particularly around flowering time), or disease and pests, these pre-flowering flights may prove less predictive of yield since the health and trajectory of the plants would be interrupted by these stressors. In this case, having more flights, or flights around times of stress, might prove more important for dissecting genotype-specific responses. Each flight throughout the season could also be viewed as representing a single, but correlated environment, increasing our confidence in the overall results but still not addressing the question of how many flights are needed to "saturate" the phenome. The answer to this question is likely dependent on many factors and additional experiments like this one across more environments would provide a set of data to evaluate the risks and benefits of higher or lower temporal density sampling. In general, the resources needed for flying each additional time point currently are much lower than the resources needed to process the resulting images into knowledge. Therefore, it is recommended to fly as frequently as possible and then choose dates for processing based on the weather or stress experienced and traits of interest.

Another limitation of this study is that only RGB VIs were used, therefore the additional phenomic features came from increasing temporal rather than spectral biomarkers. This also meant that the structure from motion PHT data was variable and noisy, requiring the use of the Weibull fit to smooth the data temporally. More accurate height estimates could be made if Light Detection and Ranging data were collected. For example, Bayesian Networks have shown promise for temporal PHT modeling from manual phenotype data and more accurate and consistent UAS PHT data would be a good candidate for use with those methods (Dos Santos et al., 2020). It is expected that multispectral, hyperspectral, or other increased spectral imaging would also increase prediction power and possibly further separate autocorrelations between dates. Additionally, the yield prediction methods here employed, and the yield phenotype itself, are end-of-season and deployed in an annual production system. In cases where within-season phenotype prediction is desired or where multiple harvests occur from the same plant (e.g., forage crops), temporally dense data may also be more informative. For scientific research into plant growth and development in the field, studies of such dense data may turn out to be highly important. Other modeling frameworks, particularly those that are more process based, such as physiological crop growth models (CGM), rely heavily on data points throughout the plant's life cycle and may also be improved by dense UAV phenotyping data, potentially even allowing them to predict end-of-season phenotypes more accurately than the methods used here. Additionally, CGMs may be used to interpolate between UAV flight dates improving the accuracy of the models and reducing and/or informing the number of flights needed.

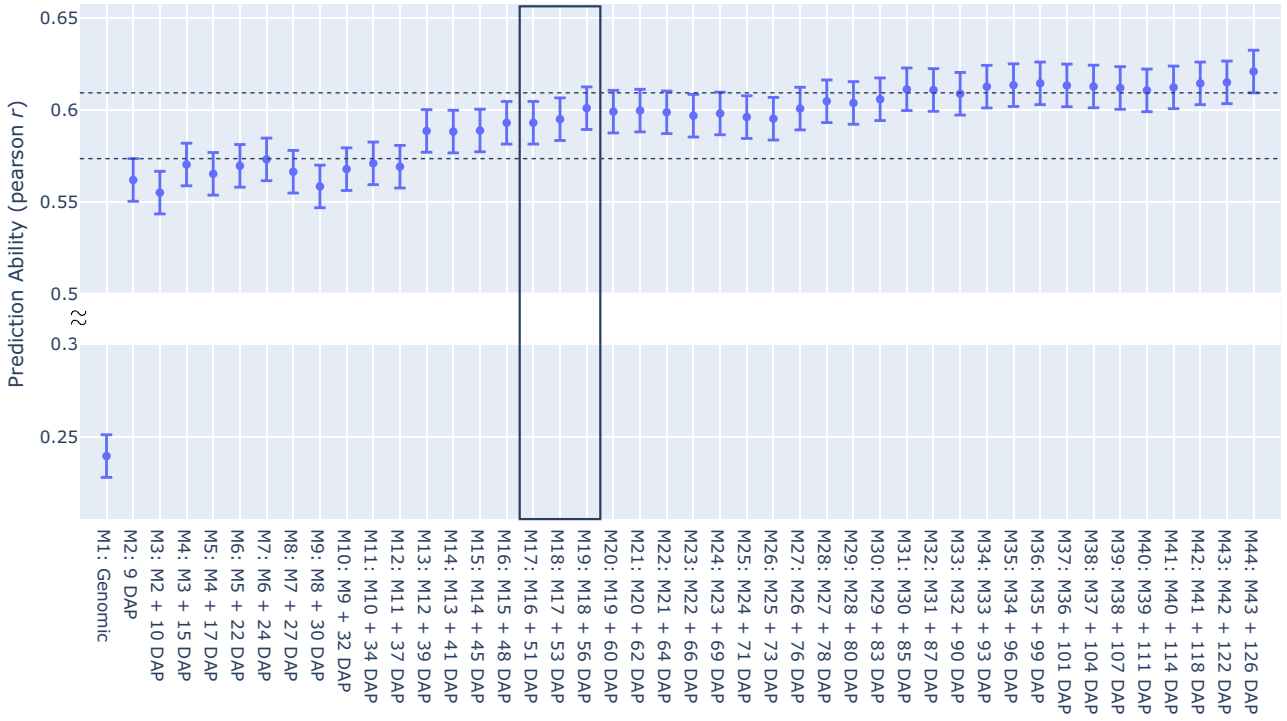

FIGURE 6 Yield prediction models including: Genomic prediction (M1) compared to phenomic prediction from the first flight date (M2), the first and second flight date (M3), and subsequent flight dates following the same pattern of adding one new flight date to each model (M4-M44). M2-M44 include all vegetative indices and plant height. Displayed values are the means and the simultaneous Tukey's HSD 95% confidence intervals for each model. Dotted lines are for ease in visualizing models that are significantly more accurate than the first flight date model (M2) and/or significantly less accurate than the last model. Average flowering time is highlighted by the box.

AUTHOR CONTRIBUTIONS

Jacob D. Washburn: Conceptualization; data curation; formal analysis; investigation; methodology; project administration; resources; supervision; visualization; writing—original draft; writing—review and editing. **Alper Adak**: Conceptualization; data curation; formal analysis; investigation; methodology; visualization; writing—original draft; writing—review and editing. **Aaron J. DeSalvio**: Data curation; formal analysis; writing—review and editing. **Mustafa A. Arik**: Data curation; formal analysis; writing—review and editing. **Seth C. Murray**: Conceptualization; writing—original draft; writing—review and editing.

ACKNOWLEDGMENTS

This research was supported by the United States Department of Agriculture, Agricultural Research Service and the Iowa Corn Promotion Board. Unoccupied aerial systems data processing support was facilitated by USDA award # 2022-70412-38454 Agriculture Genome to Phenome Initiative (AG2PI) seed grant.

CONFLICT OF INTEREST STATEMENT

The authors declare no conflicts of interest.

DATA AVAILABILITY STATEMENT

The scripts used in the analyses and figure generation for this manuscript are available at https://github.com/JacobWashburn-USDA/dense_UAV. Both the scripts and phenotypic tabular data needed to recreate the analyses are available at https://doi.org/10.5281/zenodo.11085557.

ORCID

Jacob D. Washburn https://orcid.org/0000-0003-0185-7105
Alper Adak https://orcid.org/0000-0002-2737-8041
Aaron J. DeSalvio https://orcid.org/0000-0003-1818-4699

REFERENCES

Adak, A., Anderson, S. L., & Murray, S. C. (2023). Pedigree-management-flight interaction for temporal phenotype analysis and temporal phenomic prediction. *The Plant Phenome Journal*, *6*(1), e20057. https://doi.org/10.1002/ppj2.20057

Adak, A., Murray, S. C., Anderson, S. L., Popescu, S. C., Malambo, L., Romay, M. C., & De Leon, N. (2021). Unoccupied aerial systems discovered overlooked loci capturing the variation of entire growing period in maize. *Plant Genome*, *14*(2), e20102. https://doi.org/10.1002/tpg2.20102

Adak, A., Murray, S. C., Božinović, S., Lindsey, R., Nakasagga, S., Chatterjee, S., Anderson, S. L., & Wilde, S. (2021). Temporal veg-

etation indices and plant height from remotely sensed imagery can predict grain yield and flowering time breeding value in maize via machine learning regression. *Remote Sensing*, *13*(11), 2141. https://doi.org/10.3390/rs13112141

Alkhalifah, N., Campbell, D. A., Falcon, C. M., Gardiner, J. M., Miller, N. D., Romay, M. C., Walls, R., Walton, R., Yeh, C.-T., Bohn, M., Bubert, J., Buckler, E. S., Ciampitti, I., Flint-Garcia, S., Gore, M. A., Graham, C., Hirsch, C., Holland, J. B., Hooker, D., … Lawrence-Dill, C. J. (2018). Maize genomes to fields: 2014 and 2015 field season genotype, phenotype, environment, and inbred ear image datasets. *BMC Research Notes*, *11*(1), Article 452. https://doi.org/10.1186/s13104-018-3508-1

Amadeu, R. R., Cellon, C., Olmstead, J. W., Garcia, A. A. F., Resende, M. F. R., & Muñoz, P. R. (2016). AGHmatrix: R package to construct relationship matrices for autotetraploid and diploid species: A blueberry example. *Plant Genome*, *9*(3), plantgenome2016.01.0009. https://doi.org/10.3835/plantgenome2016.01.0009

Anderson, S. L., & Murray, S. C. (2020). R/UAStools::plotshpcreate: Create multi-polygon shapefiles for extraction of research plot scale agriculture remote sensing data. *Frontiers in Plant Science*, *11*, Article 511768. https://doi.org/10.3389/fpls.2020.511768

Anderson, S. L., Murray, S. C., Chen, Y., Malambo, L., Chang, A., Popescu, S., Cope, D., & Jung, J. (2020). Unoccupied aerial system enabled functional modeling of maize height reveals dynamic expression of loci. *Plant Direct*, *4*(5), e00223. https://doi.org/10.1002/pld3.223

Anderson, S. L., Murray, S. C., Malambo, L., Ratcliff, C., Popescu, S., Cope, D., Chang, A., Jung, J., & Thomasson, J. A (2019). Prediction of maize grain yield before maturity using improved temporal height estimates of unmanned aerial systems. *The Plant Phenome Journal*, *2*(1), 1–15. https://doi.org/10.2135/tppj2019.02.0004

Araus, J. L., & Cairns, J. E. (2014). Field high-throughput phenotyping: The new crop breeding frontier. *Trends in Plant Science*, *19*(1), 52–61. https://doi.org/10.1016/j.tplants.2013.09.008

Bendig, J., Yu, K., Aasen, H., Bolten, A., Bennertz, S., Broscheit, J., Gnyp, M. L., & Bareth, G. (2015). Combining UAV-based plant height from crop surface models, visible, and near infrared vegetation indices for biomass monitoring in barley. *International Journal of Applied Earth Observation and Geoinformation*, *39*, 79–87.

Burgos-Artizzu, X. P., Ribeiro, A., Guijarro, M., & Pajares, G. (2011). Real-time image processing for crop/weed discrimination in maize fields. *Computers and Electronics in Agriculture*, *75*(2), 337–346. https://doi.org/10.1016/j.compag.2010.12.011

Burgueño, J., de los Campos, G., Weigel, K., & Crossa, J. (2012). Genomic prediction of breeding values when modeling genotype × environment interaction using pedigree and dense molecular markers. *Crop Science*, *52*, 707–719. https://doi.org/10.2135/cropsci2011.06.0299

Danilevicz, M. F., Bayer, P. E., Boussaid, F., Bennamoun, M., & Edwards, D. (2021). Maize yield prediction at an early developmental stage using multispectral images and genotype data for preliminary hybrid selection. *Remote Sensing*, *13*(19), 3976. https://doi.org/10.3390/rs13193976

de los Campos, G., Gianola, D., & Rosa, G. J. M. (2009). Reproducing kernel Hilbert spaces regression: A general framework for genetic evaluation. *Journal of Animal Science*, *87*(6), 1883–1887. https://doi.org/10.2527/jas.2008-1259

Dos Santos, J. P. R., Fernandes, S. B., Mccoy, S., Lozano, R., Brown, P. J., Leakey, A. D. B., Buckler, E. S., Garcia, A. A. F., & Gore, M. A. (2020). Novel bayesian networks for genomic prediction of developmental traits in biomass sorghum. *G3 Genes|Genomes|Genetics*, *10*(2), 769–781. https://doi.org/10.1534/g3.119.400759

Fahlgren, N., Feldman, M., Gehan, M. A., Wilson, M. S., Shyu, C., Bryant, D. W., Hill, S. T., Mcentee, C. J., Warnasooriya, S. N., Kumar, I., Ficor, T., Turnipseed, S., Gilbert, K. B., Brutnell, T. P., Carrington, J. C., Mockler, T. C., & Baxter, I. (2015). A versatile phenotyping system and analytics platform reveals diverse temporal responses to water availability in *Setaria*. *Molecular Plant*, *8*(10), 1520–1535. https://doi.org/10.1016/j.molp.2015.06.005

Gage, J. L., Jarquin, D., Romay, C., Lorenz, A., Buckler, E. S., Kaeppler, S., Alkhalifah, N., Bohn, M., Campbell, D. A., Edwards, J., Ertl, D., Flint-Garcia, S., Gardiner, J., Good, B., Hirsch, C. N., Holland, J., Hooker, D. C., Knoll, J., Kolkman, J., … De Leon, N. (2017). The effect of artificial selection on phenotypic plasticity in maize. *Nature Communications*, *8*(1), Artcle 1348. https://doi.org/10.1038/s41467-017-01450-2

Gitelson, A. A., Kaufman, Y. J., Stark, R., & Rundquist, D. (2002). Novel algorithms for remote estimation of vegetation fraction. *Remote Sensing of Environment*, *80*(1), 76–87. https://doi.org/10.1016/S0034-4257(01)00289-9

Golzarian, M. R., & Frick, R. A. (2011). Classification of images of wheat, ryegrass and brome grass species at early growth stages using principal component analysis. *Plant Methods*, *7*(1), Article 28. https://doi.org/10.1186/1746-4811-7-28

Guerrero, J. M., Pajares, G., Montalvo, M., Romeo, J., & Guijarro, M. (2012). Support vector machines for crop/weeds identification in maize fields. *Expert Systems with Applications*, *39*(12), 11149–11155. https://doi.org/10.1016/j.eswa.2012.03.040

Guijarro, M., Pajares, G., Riomoros, I., Herrera, P. J., Burgos-Artizzu, X. P., & Ribeiro, A. (2011). Automatic segmentation of relevant textures in agricultural images. *Computers and Electronics in Agriculture*, *75*(1), 75–83. https://doi.org/10.1016/j.compag.2010.09.013

Hague, T., Tillett, N. D., & Wheeler, H. (2006). Automated crop and weed monitoring in widely spaced cereals. *Precision Agriculture*, *7*(1), 21–32. https://doi.org/10.1007/s11119-005-6787-1

Herr, A. W., Adak, A., Carroll, M. E., Elango, D., Kar, S., Li, C., Jones, S. E., Carter, A. H., Murray, S. C., Paterson, A., Sankaran, S., Singh, A., & Singh, A. K. (2023). UAS imagery for phenotyping in cotton, maize, soybean, and wheat breeding. *Crop Science*, *63*, 1722–1749. https://doi.org/10.1002/csc2.21028

Hochberg, Y., & Tamhane, A. (2009). *Multiple comparison procedures*. John Wiley & Sons.

Hunt, E. R., Cavigelli, M., Daughtry, C. S. T., Mcmurtrey, J. E., & Walthall, C. L. (2005). Evaluation of digital photography from model aircraft for remote sensing of crop biomass and nitrogen status. *Precision Agriculture*, *6*(4), 359–378. https://doi.org/10.1007/s11119-005-2324-5

Hunt, E. R., Daughtry, C. S. T., Eitel, J. U. H., & Long, D. S. (2011). Remote sensing leaf chlorophyll content using a visible band index. *Agronomy Journal*, *103*(4), 1090–1099. https://doi.org/10.2134/agronj2010.0395

Kataoka, T., Kaneko, T., Okamoto, H., & Hata, S. (2004). Crop growth estimation system using machine vision. In *Proceedings 2003 IEEE/ASME international conference on advanced intelligent mechatronics (AIM 2003)* (pp. b1079–b1083). IEEE.

Kick, D. R., Wallace, J. G., Schnable, J. C., Kolkman, J. M., Alaca, B., Beissinger, T. M., Edwards, J., Ertl, D., Flint-Garcia, S., Gage, J. L., Hirsch, C. N., Knoll, J. E., De Leon, N., Lima, D. C.,

Moreta, D. E., Singh, M. P., Thompson, A., Weldekidan, T., & Washburn, J. D. (2023). Yield prediction through integration of genetic, environment, and management data through deep learning. *G3 Genes|Genomes|Genetics*, *13*(4), jkad006. https://doi.org/10.1093/g3journal/jkad006

Krause, M. R., González-Pérez, L., Crossa, J., Pérez-Rodríguez, P., Montesinos-López, O., Singh, R. P., Dreisigacker, S., Poland, J., Rutkoski, J., Sorrells, M., Gore, M. A., & Mondal, S. (2019). Hyperspectral reflectance-derived relationship matrices for genomic prediction of grain yield in wheat. *G3 Genes|Genomes|Genetics*, *9*(4), 1231–1247. https://doi.org/10.1534/g3.118.200856

Lawrence-Dill, C. J., Schnable, P. S., & Springer, N. M. (2019). Idea factory: The maize genomes to fields initiative. *Crop Science*, *59*(4), 1406–1410. https://doi.org/10.2135/cropsci2019.02.0071

Lima, D. C., Aviles, A. C., Alpers, R. T., Mcfarland, B. A., Kaeppler, S., Ertl, D., Romay, M. C., Gage, J. L., Holland, J., Beissinger, T., Bohn, M., Buckler, E., Edwards, J., Flint-Garcia, S., Hirsch, C. N., Hood, E., Hooker, D. C., Knoll, J. E., Kolkman, J. M., … De Leon, N. (2023). 2018–2019 field seasons of the maize genomes to fields (G2F) G x E project. *BMC Genomic Data*, *24*(1), Article 29. https://doi.org/10.1186/s12863-023-01129-2

Lima, D. C., Aviles, A. C., Alpers, R. T., Perkins, A., Schoemaker, D. L., Costa, M., Michel, K. J., Kaeppler, S., Ertl, D., Romay, M. C., Gage, J. L., Holland, J., Beissinger, T., Bohn, M., Buckler, E., Edwards, J., Flint-Garcia, S., Gore, M. A., Hirsch, C. N., … De Leon, N. (2023). 2020–2021 field seasons of Maize G x E project within the genomes to fields initiative. *BMC Research Notes*, *16*(1), Article 219. https://doi.org/10.1186/s13104-023-06430-y

Lima, D. C., Washburn, J. D., Varela, J. I., Chen, Q., Gage, J. L., Romay, M. C., Holland, J., Ertl, D., Lopez-Cruz, M., Aguate, F. M., de los Campos, G., Kaeppler, S., Beissinger, T., Bohn, M., Buckler, E., Edwards, J., Flint-Garcia, S., Gore, M. A., Hirsch, C. N., … De Leon, N. (2023). Genomes to fields 2022 maize genotype by environment prediction competition. *BMC Research Notes*, *16*(1), Article 148. https://doi.org/10.1186/s13104-023-06421-z

Louhaichi, M., Borman, M. M., & Johnson, D. E. (2001). Spatially located platform and aerial photography for documentation of grazing impacts on wheat. *Geocarto International*, *16*(1), 65–70. https://doi.org/10.1080/10106040108542184

Ma, B. L., Dwyer, L. M., Costa, C., Cober, E. R., & Morrison, M. J. (2001). Early prediction of soybean yield from canopy reflectance measurements. *Agronomy Journal*, *93*(6), 1227–1234. https://doi.org/10.2134/agronj2001.1227

Matias, F. I., Caraza-Harter, M. V., & Endelman, J. B. (2020). FIELDimageR: An R package to analyze orthomosaic images from agricultural field trials. *The Plant Phenome Journal*, *3*(1), e20005. https://doi.org/10.1002/ppj2.20005

Mcfarland, B. A., Alkhalifah, N., Bohn, M., Bubert, J., Buckler, E. S., Ciampitti, I., Edwards, J., Ertl, D., Gage, J. L., Falcon, C. M., Flint-Garcia, S., Gore, M. A., Graham, C., Hirsch, C. N., Holland, J. B., Hood, E., Hooker, D., Jarquin, D., Kaeppler, S. M., … de Leon, N. (2020). Maize genomes to fields (G2F): 2014–2017 field seasons: Genotype, phenotype, climatic, soil, and inbred ear image datasets. *BMC Research Notes*, *13*(1), Article 71. https://doi.org/10.1186/s13104-020-4922-8

Messina, C. D., Hammer, G. L., Mclean, G., Cooper, M., van Oosterom, E. J., Tardieu, F., Chapman, S. C., Doherty, A., & Gho, C. (2019). On the dynamic determinants of reproductive failure under drought in maize. *In Silico Plants*, *1*(1), diz003. https://doi.org/10.1093/insilicoplants/diz003

Messina, C. D., Podlich, D., Dong, Z., Samples, M., & Cooper, M. (2011). Yield–trait performance landscapes: From theory to application in breeding maize for drought tolerance. *Journal of Experimental Botany*, *62*(3), 855–868. https://doi.org/10.1093/jxb/erq329

Meyer, G. E., Hindman, T. W., & Laksmi, K. (1999). Machine vision detection parameters for plant species identification. In G. E. Meyer & J. A. DeShazer (Eds.), *Precision agriculture and biological quality* (Vol. 3543, pp. 327–335). SPIE.

Meyer, G. E., & Neto, J. C. (2008). Verification of color vegetation indices for automated crop imaging applications. *Computers and Electronics in Agriculture*, *63*(2), 282–293. https://doi.org/10.1016/j.compag.2008.03.009

Murray, S. C., Adak, A., Desalvio, A., & Lane, H. (2022). Temporal field phenomics allows discovery of nature AND nurture, so can we saturate the phenome? *Authorea*. https://doi.org/10.22541/au.166758437.79328391/v1

Mutka, A. M., & Bart, R. S. (2015). Image-based phenotyping of plant disease symptoms. *Frontiers in Plant Science*, *5*, Article 734. https://doi.org/10.3389/fpls.2014.00734

Oehme, L. H., Reineke, A.-J., Weiß, T. M., Würschum, T., He, X., & Müller, J. (2022). Remote sensing of maize plant height at different growth stages using UAV-based digital surface models (DSM). *Agronomy*, *12*(4), 958. https://doi.org/10.3390/agronomy12040958

Reynolds, M., & Langridge, P. (2016). Physiological breeding. *Current Opinion in Plant Biology*, *31*, 162–171. https://doi.org/10.1016/j.pbi.2016.04.005

Richardson, A. J., & Wiegand, C. (1977). Distinguishing vegetation from soil background information. *Photogrammetric Engineering and Remote Sensing*, *43*, 1541–1552.

Rogers, A. R., Dunne, J. C., Romay, C., Bohn, M., Buckler, E. S., Ciampitti, I. A., Edwards, J., Ertl, D., Flint-Garcia, S., Gore, M. A., Graham, C., Hirsch, C. N., Hood, E., Hooker, D. C., Knoll, J., Lee, E. C., Lorenz, A., Lynch, J. P., Mckay, J., … Holland, J. B. (2021). The importance of dominance and genotype-by-environment interactions on grain yield variation in a large-scale public cooperative maize experiment. *G3 Genes|Genomes|Genetics*, *11*(2), jkaa050. https://doi.org/10.1093/g3journal/jkaa050

Rutkoski, J., Poland, J., Mondal, S., Autrique, E., Pérez, L. G., Crossa, J., Reynolds, M., & Singh, R. (2016). Canopy temperature and vegetation indices from high-throughput phenotyping improve accuracy of pedigree and genomic selection for grain yield in wheat. *G3 Genes|Genomes|Genetics*, *6*(9), 2799–2808. https://doi.org/10.1534/g3.116.032888

Shi, Y., Thomasson, J. A., Murray, S. C., Pugh, N. A., Rooney, W. L., Shafian, S., Rajan, N., Rouze, G., Morgan, C. L. S., Neely, H. L., Rana, A., Bagavathiannan, M. V., Henrickson, J., Bowden, E., Valasek, J., Olsenholler, J., Bishop, M. P., Sheridan, R., Putman, E. B., … Yang, C. (2016). Unmanned aerial vehicles for high-throughput phenotyping and agronomic research. *PLoS One*, *11*(7), e0159781. https://doi.org/10.1371/journal.pone.0159781

Singh, D., Wang, X., Kumar, U., Gao, L., Noor, M., Imtiaz, M., Singh, R. P., & Poland, J. (2019). High-throughput phenotyping enabled genetic dissection of crop lodging in wheat. *Frontiers in Plant Science*, *10*, Article 394. https://doi.org/10.3389/fpls.2019.00394

Sweet, D. D., Tirado, S. B., Springer, N. M., Hirsch, C. N., & Hirsch, C. D. (2022). Opportunities and challenges in phenotyping row crops

using drone-based RGB imaging. *The Plant Phenome Journal*, *5*(1), e20044. https://doi.org/10.1002/ppj2.20044

Tirado, S. B., Hirsch, C. N., & Springer, N. M. (2021). Utilizing temporal measurements from UAVs to assess root lodging in maize and its impact on productivity. *Field Crops Research*, *262*, 108014. https://doi.org/10.1016/j.fcr.2020.108014

Tucker, C. J. (1979). Red and photographic infrared linear combinations for monitoring vegetation. *Remote Sensing of Environment*, *8*(2), 127–150. https://doi.org/10.1016/0034-4257(79)90013-0

Vanraden, P. M. (2008). Efficient methods to compute genomic predictions. *Journal of Dairy Science*, *91*(11), 4414–4423. https://doi.org/10.3168/jds.2007-0980

Vitezica, Z. G., Varona, L., & Legarra, A. (2013). On the additive and dominant variance and covariance of individuals within the genomic selection scope. *Genetics*, *195*(4), 1223–1230. https://doi.org/10.1534/genetics.113.155176

Wang, X., Zhang, R., Song, W., Han, L., Liu, X., Sun, X., Luo, M., Chen, K., Zhang, Y., Yang, H., Yang, G., Zhao, Y., & Zhao, J. (2019). Dynamic plant height QTL revealed in maize through remote sensing phenotyping using a high-throughput unmanned aerial vehicle (UAV). *Scientific Reports*, *9*(1), Article 3458.

Washburn, J. D., Cimen, E., Ramstein, G., Reeves, T., O'briant, P., Mclean, G., Cooper, M., Hammer, G., & Buckler, E. S. (2021). Predicting phenotypes from genetic, environment, management, and historical data using CNNs. *Theoretical and Applied Genetics*, *134*(12), 3997–4011. https://doi.org/10.1007/s00122-021-03943-7

Woebbecke, D. M., Meyer, G. E., Von Bargen, K., & Mortensen, D. A. (1995). Color indices for weed identification under various soil, residue, and lighting conditions. *Transactions of the ASAE*, *38*(1), 259–269. https://doi.org/10.13031/2013.27838

Yuan, W., Wijewardane, N. K., Jenkins, S., Bai, G., Ge, Y., & Graef, G. L. (2019). Early prediction of soybean traits through color and texture features of canopy RGB imagery. *Scientific Reports*, *9*(1), Article 14089. https://doi.org/10.1038/s41598-019-50480-x

Zarcotejada, P., Berjon, A., Lopezlozano, R., Miller, J., Martin, P., Cachorro, V., Gonzalez, M., & Defrutos, A. (2005). Assessing vineyard condition with hyperspectral indices: Leaf and canopy reflectance simulation in a row-structured discontinuous canopy. *Remote Sensing of Environment*, *99*(3), 271–287. https://doi.org/10.1016/j.rse.2005.09.002

Zhang, L., Niu, Y., Zhang, H., Han, W., Li, G., Tang, J., & Peng, X. (2019). Maize canopy temperature extracted from UAV thermal and RGB imagery and its application in water stress monitoring. *Frontiers in Plant Science*, *10*, Article 1270. https://doi.org/10.3389/fpls.2019.01270

Zhang, M., Qin, Z., Liu, X., & Ustin, S. L. (2003). Detection of stress in tomatoes induced by late blight disease in California, USA, using hyperspectral remote sensing. *International Journal of Applied Earth Observation and Geoinformation*, *4*(4), 295–310.

SUPPORTING INFORMATION

Additional supporting information can be found online in the Supporting Information section at the end of this article.

How to cite this article: Washburn, J. D., Adak, A., DeSalvio, A. J., Arik, M. A., & Murray, S. C. (2024). High temporal resolution unoccupied aerial systems phenotyping provides unique information between flight dates. *The Plant Phenome Journal*, *7*, e20113. https://doi.org/10.1002/ppj2.20113